ChemBioChem

Research Article
doi.org/10.1002/cbic.202200713

Chemistry Europe
European Chemical Societies Publishing

www.chembiochem.org

Novel Approach for the Isolation and Immobilization of a Recombinant Transaminase: Applying an Advanced Nanocomposite System

Gábor Koplányi,[a] Evelin Bell,[a] Zsófia Molnár,[a, b] Gábor Katona,[c] Péter Lajos Neumann,[d, e] Ferenc Ender,[d, f] György T. Balogh,[g, h] Polona Žnidaršič-Plazl,[i] László Poppe,[a, j] and Diána Balogh-Weiser*[a, k]

The increasing application of recombinant enzymes demands not only effective and sustainable fermentation, but also highly efficient downstream processing and further stabilization of the enzymes by immobilization. In this study, a novel approach for the isolation and immobilization of His-tagged transaminase from *Chromobacterium violaceum* (*Cv*TA) has been developed. A recombinant of *Cv*TA was simultaneously isolated and immobilized by binding on silica nanoparticles (SNPs) with metal affinity linkers and additionally within poly(lactic acid) (PLA) nanofibers. The linker length and the nature of the metal ion significantly affected the enzyme binding efficiency and biocatalytic activity of *Cv*TA-SNPs. The formation of PLA nanofibers by electrospinning enabled rapid embedding of *Cv*TA-SNPs biocatalysts and ensured enhanced stability and activity. The developed advanced immobilization method reduces the time required for enzyme isolation, purification and immobilization by more than fourfold compared to a classical stepwise technique.

Introduction

The demand for industrial applications of enzymes has led to a continuous development of biotechnology and enzyme-catalyzed industrial reactions since the nineteenth century.[1] Nowadays, enzymes are used in many industries, such as pulp and paper production,[2] food industry,[3] pharmaceutical industry,[4] and biofuel production.[5] In addition, their use in medical diagnostics and as biopharmaceuticals continues to expand.[6,7] At the same time, heterologous expression systems and protein engineering strategies, such as directed evolution and point mutations, enabled the production of recombinant enzymes with improved performance and high-level catalytic activity. In addition, the new approaches enabled the production of tailored enzymes for a desired process.[8] Today's biotechnology offers a comprehensive arsenal of powerful approaches to discover, improve, and use enzymes to produce value-added compounds.[9]

Transaminases or aminotransferases (EC 2.6.1.X) from the transferase enzymes class mediate the transfer of a primary amino group to the oxo group of ketone compounds in the presence of the coenzyme pyridoxal-5′-phosphate. In the

[a] G. Koplányi, Dr. E. Bell, Dr. Z. Molnár, Prof. Dr. L. Poppe, Dr. D. Balogh-Weiser
Department of Organic Chemistry and Technology
Budapest University of Technology and Economics
1111, Műegyetem rkp. 3. Budapest (Hungary)
E-mail: balogh.weiser.diana@vbk.bme.hu
[b] Dr. Z. Molnár
Institute of Enzymology
ELKH Research Center of Natural Sciences
1117 Magyar tudosók krt. 2. Budapest (Hungary)
[c] Dr. G. Katona
Institute of Pharmaceutical Technology and Regulatory Affairs
University of Szeged
6720, Eötvös u. 6. Szeged (Hungary)
[d] Dr. P. Lajos Neumann, Dr. F. Ender
Department of Electron Devices
Budapest University of Technology and Economics
1111, Műegyetem rkp. 3. Budapest (Hungary)
[e] Dr. P. Lajos Neumann
Centre for Energy Research
Institute for Technical Physics and Materials Science
1121, Konkoly-Thege M. út 29–33. Budapest (Hungary)
[f] Dr. F. Ender
SpinSplit Llc.
1025, Vend u. 17. Budapest (Hungary)
[g] Prof. Dr. G. T. Balogh
Department of Chemical and Environmental Process Engineering
Budapest University of Technology and Economics
1111, Műegyetem rkp. 3. Budapest (Hungary)
[h] Prof. Dr. G. T. Balogh
Institute of Pharmacodynamics and Biopharmacy
University of Szeged
6720, Eötvös u. 6. Szeged (Hungary)
[i] Prof. Dr. P. Žnidaršič-Plazl
Faculty of Chemistry and Chemical Technology
University of Ljubljana
Večna pot 113. 1000 Ljubljana (Slovenia)
[j] Prof. Dr. L. Poppe
Biocatalysis and Biotransformation Research Center
Faculty of Chemistry and Chemical Engineering
Babeş-Bolyai University of Cluj-Napoca
400028, Arany János Str. 11, Cluj-Napoca (Romania)
[k] Dr. D. Balogh-Weiser
Department of Physical Chemistry and Materials Science
Budapest University of Technology and Economics
1111, Műegyetem rkp. 3. Budapest (Hungary)

human body, aspartate aminotransferase (AST) and alanine aminotransferase (ALT) are located in the liver and are responsible for metabolizing excess amino acids in the blood. This makes them a commonly used marker in the diagnostics of liver and other gastrointestinal diseases.[10] In recent years, the application of transaminases (TAs) has gained interest as promising biocatalysts that provide an environmentally friendly route for the synthesis of pharmaceutically relevant chiral amines with high stereoselectivity and catalytic turnover.[11–13] The ω-TAs are the most common natural enzymes that can directly synthesize enantiopure chiral amines by asymmetric amination of prochiral ketones or by kinetic resolution of the racemic mixture of amines.[14]

Purification processes in protein engineering have a crucial role to obtain pure recombinant enzymes with high-level activity. Mostly immobilized metal ion affinity chromatography (IMAC) is used to perform the selective isolation of the target proteins constructed with different types of affinity tags such as His-tag, GST-tag, HaloTag etc.[15] In the case of another well-known alternative called the SpyTag-SpyCatcher technique, irreversible site-specific isopeptide bonds are formed between the SpyTag of the target and the SpyCatcher protein.[16,17] However, in most cases the purified enzymes retain their activity, these purification methods are rather considered time consuming and less cost-effective from this perspective compared to the single-step isolation.[18,19] Thus, all of these contributes to the development of novel chemically modified nanomaterials combining the previously mentioned methods to perform single-step purification processes.[20–22] One of these new generation nanomaterials, the hybrid nanoflowers showed great potential in the field of protein immobilization. Recently, it was reported that nanoflowers formed by Cu^{2+} ions incorporated enzymes exhibited enhanced activity, stability and reusability after four cycles.[23–25]

Nanoparticles also have several advantageous properties such as large surface area to volume ratio, improved optical, mechanical, and functional characteristics.[26] These distinct and significant characteristics resulted in their application in various fields such as food industries and packaging, nanomedicines for clinical use, composite systems etc.[26–28] Furthermore, silica nanoparticles (SNPs) have great potential due to their ability to form uniform mesopores, their controllable morphology, potential surface functionalization, and biocompatibility.[29] Several types of SNPs such as spherical monodispersed, mesoporous,[30] hollow core-shell,[31] and rod-like[32] structures can be prepared depending on their final application. Commonly, SNPs are prepared by the sol-gel, or by the so-called Stöber modification method with the control of reactant to solvent ratio, or the application of surfactants and templates to control the particle size and final morphology.[33] To even broaden the application of SNPs, their physical and chemical properties are modified by the generation of composite materials either by embedment or crosslinking.[34] In the latter case, functionalized SNPs with reactive functional groups on the surfaces are crosslinked by bifunctional agents like glutaraldehyde or organosilane compounds forming reinforced network material.[35–37] On the other hand, entrapment or embedment in polymer matrices are more common in the preparation of fibrous composite materials. Electrospinning technique has recently attracted great attention in preparation of nanofibrous composite materials to entrap functionalized SNPs in biocompatible synthetic polymers such as poly(ε-caprolactone) (PCL),[38] poly(lactic acid) (PLA),[39] and poly(lactic-co-glycolic acid) (PLGA)[40] for food packaging or tissue engineering applications. PLA is an environmentally friendly, commercially available, inexpensive material with good thermal stability and high chemical resistance against water and several solvents such as, alcohols, aromatic and aliphatic organic solvents at ambient conditions.[41,42] Furthermore, uniform and defect-free nanofibrous matrices can be prepared from PLA by solvent-based electrospinning process.[43]

The aim of this study was to develop a suitable method for simultaneous purification and immobilization of the recombinant *Chromobacterium violaceum* transaminase (*Cv*TA) expressed in *Escherichia coli* using functionalized SNPs and further immobilization in a novel nanofibrous composite biocatalyst. For this purpose, SNPs were functionalized by specific affinity linkers that allow complexation of metal ions on the surface. Such nanocarrier systems were tested for the selective isolation of the target *Cv*TA enzyme labeled by the hexahistidine tag from the highly complex environment.[44] Moreover, our target was the entrapment of enzyme-covered nanoparticles in PLA nanomatrices by emulsion electrospinning technique The characterization of particle size distribution of generated SNPs was performed by DLS measurements, while the morphology of functionalized SNPs and composite nanofibers was investigated by electron microscopy. The biocatalytic performance of the immobilized *Cv*TA was characterized by the oxidative deamination of (*S*)-(−)-α-methylbenzylamine [(*S*)-MBA] to acetophenone by UV-Vis spectrophotometry. According to our best knowledge, this is the first report on application of nanoparticles with metal ion affinity and polymeric nanofibers for the combined isolation, immobilization and thereby stabilization of a recombinant enzyme.

Results and Discussion

To isolate the His-tagged *Cv*TA, silica nanoparticles were functionalized with specific affinity linkers of various chain lengths (Figure 1). As a result, coordinative binding interaction was formed between the surface-functionalized SNPs and the His tag of the enzyme in the presence of the immobilized metal ion and ethylenediaminetetraacetic dianhydride (Eda) as a chelator.

To investigate the successfulness of metal complexation, the elemental analysis of the different SNP carriers had been performed by scanning electron microscope coupled energy dispersive X-ray analyzer (SEM-EDX). Results showed that, the metal loading of the nanoparticles can be realized in all cases of SNPs (Figure 2). The atomic concentration of C, N elements are mainly coming from the linkers of the particles, Si and O from SiO_2 scaffold are similarly in each case. The expected metal element was detectable at the proper metal loaded SNPs, other metal or elements were at negligible amount (< 0.005 %). In the

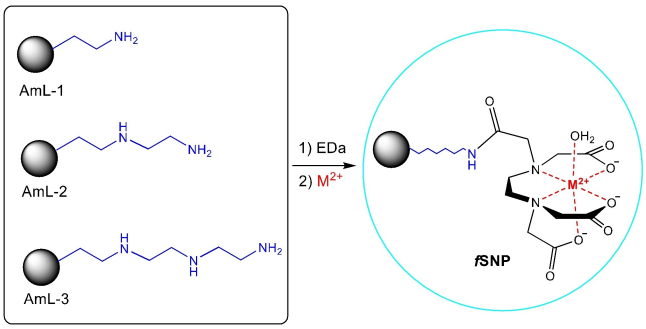

Figure 1. The principle of the interaction between the enzyme and SNPs. Amino-functionalized SNPs (*f*SNPs) were prepared by applying various aminosilanes (AmL-1, AmL-2 and AmL-3), EDa as a chelator, and a metal ion (M^+) to ensure the coordinative binding of *f*SNPs with His-tagged *Cv*TA.

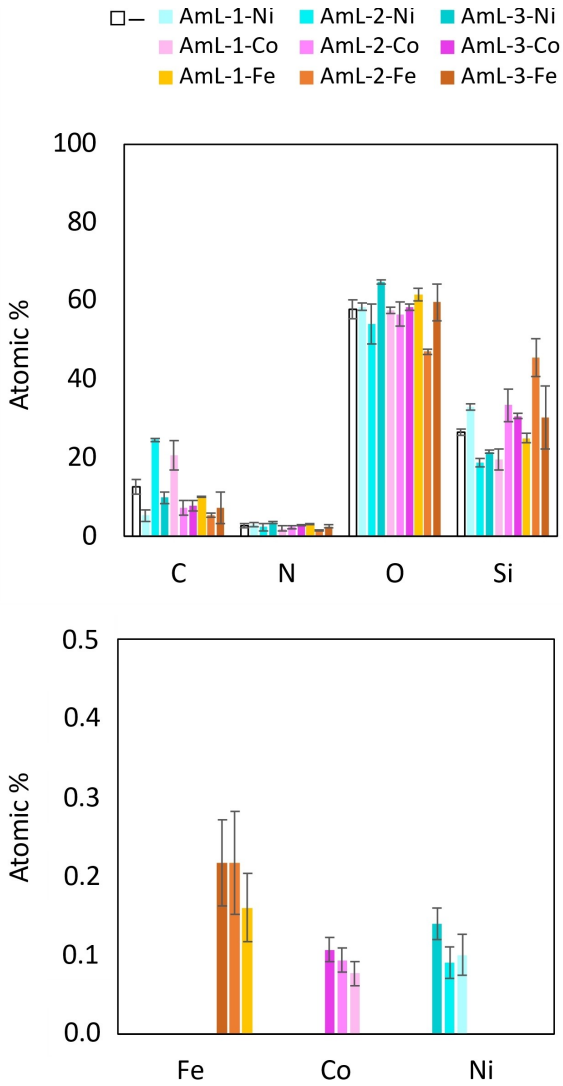

Figure 2. Element analysis of different metal (Ni, Co and Fe)-loaded silica nanoparticles (SNPs) functionalized with different amino linkers (AmL-1, AmL-2, or AmL-3) and EDa.

case of Co and Ni loaded SNPs, Ni and Co are also in the same concentration range, Fe content of Fe loaded SNPs is slightly higher, which can be caused by some precipitation of Fe precursor salt.

To compare the effect of variously modified SNPs using different linkers and metal ions on immobilization efficiency, the immobilization yield (Y_I; Figure 3a), and the activity recovery (Figure 3b) of the immobilized enzyme was evaluated for the purified enzyme and for the cell lysate. The results presented on Figure 3 indicate that the applied amino linkers had moderate effect on immobilization. On the other hand, the applied metal ion had crucial effect on the efficiency of the immobilization process. As evident from Figure 3a, nickel ion proved to be the most effective for binding with all tested amino linkers, followed by cobalt-ion functionalized SNPs, while iron(III) ion gave the lowest immobilization yield for all tested amino linkers. Regarding the specific enzyme activities (U_E, U g^{-1} which shows the amount of converted substrate to product in μmol per minute × g enzyme), all immobilized *Cv*TA biocatalysts had lower activity (U_E = 71.5 ± 3.0, 88.8 ± 25.0 and 85.2 ± 7.2 U g^{-1} for AmL-1, AmL-2 and AmL-3, respectively, in the case of Ni, U_E = 234.2 ± 35.8, 236.0 ± 35.2) and 274.8 ± 17.3 U g^{-1} for AmL-1, AmL-2 and AmL-3, respectively, in the case of Co, U_E = 34.6 ± 3.0, 57.8 ± 34.6 and 27.4 ± 24.4 U g^{-1} for AmL-1, AmL-2 and AmL-3, respectively, in the case of Fe) than the native

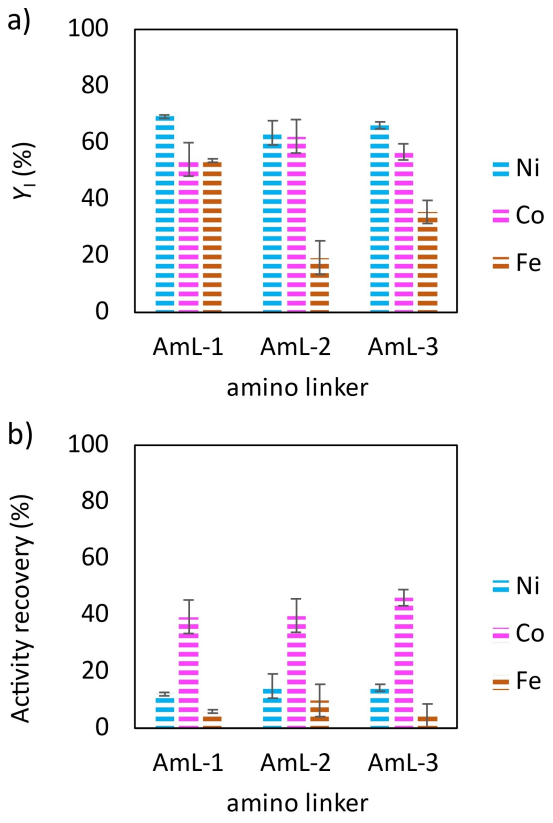

Figure 3. The effect of amino linker (AmL-1, AmL-2 and AmL-3) and metal ion (Ni, Co and Fe) of fSNPs on a) the immobilization yield (Y_I) and b) the activity recovery of the immobilized enzyme starting from purified CvTA solution.

purified *Cv*TA ($U_E = 596.0 \pm 294.0$ U g^{-1}). Iron(III) ion also resulted in the lowest activity recovery values of the immobilized enzyme, while the best activity was observed with cobalt (Figure 3b).

The specific immobilized biocatalyst activity (U_B) was determined after the immobilization of *Cv*TA on *f*SNPs either after Ni-Nitriloacetic acid (NTA) purification or directly from the crude cell lysate (Figure 4). Again, the applied amino linker had almost no effect on U_B, while significant differences were observed using various metal ions. The *Cv*TA bound to nickel-ion charged SNPs exhibited the highest U_B after immobilization from the purified *Cv*TA solution, cobalt-ion charged SNPs were just slightly less active, while iron(III)-ion functionalized SNPs led to much less active preparations (Figure 4a). Unexpectedly, the selective binding of *Cv*TA from the crude cell lysate resulted in remarkably higher U_B values than from Ni-NTA purified *Cv*TA solution. In these cases, the U_B of *Cv*TA bound to nickel and cobalt ion charged SNPs were nearly equal, while iron(III) ion again gave the lowest U_B (Figure 4b). These results indicated that the time-consuming and costly downstream process for enzyme production by recombinant protein expression could be simplified by applying surface-functionalized SNPs to perform selective isolation of the His-tagged target proteins by a single binding-centrifugation process. According to the results discussed above, the cobalt- and nickel-ion-loaded SNPs with AmL-2 or AmL-3 were similarly efficient carriers for the immobilization of *Cv*TA (>60%, $Y_I = 63.5 \pm 14.7$% for Ni and $Y_I = 62.1 \pm 4.7$% for Co with AmL-2 and, $Y_I = 66.2 \pm 10.8$% for Ni and $Y_I = 56.6.1 \pm 4.9$% for Co with AmL-3). In addition, higher specific immobilized biocatalyst activity (>12 U g^{-1}, $U_B = 13.9 \pm 0.3$% for Ni and $U_B = 13.7 \pm 0.3$% for Co with AmL-2) were observed in the case of cell lysate than with purified enzyme applying Ni or Co metal ions as well. Thus, for further investigations, the AmL-2-Co carrier was selected due to the lower production cost, considering environmental effects and toxicity, the application of Co ion was preferred over Ni compounds.[42–44]

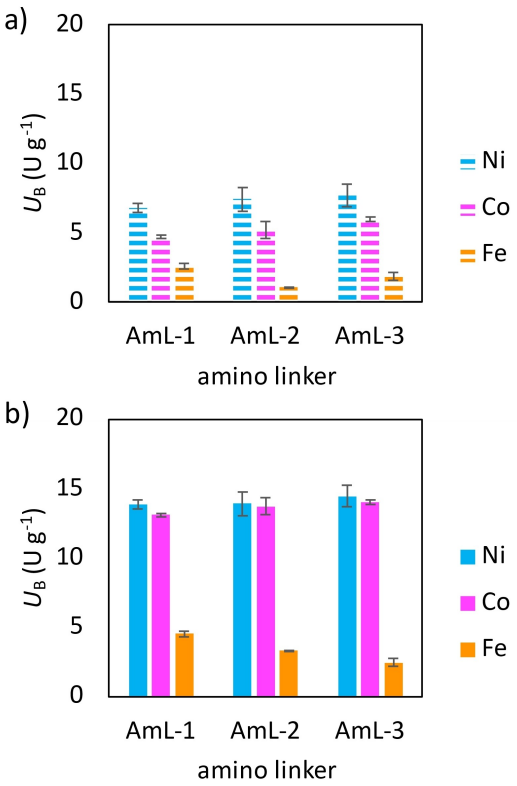

Figure 4. The effect of amino linker (AmL-1, AmL-2 or AmL-3) and metal ion (Ni, Co or Fe) on the specific immobilized biocatalytic activity UB of the fSNP-CvTA from a) purified enzyme solution and b) the cell lysate.

To characterize the cobalt-functionalized SNPs both with and without bound *Cv*TA, the average particle size (d_P) and zeta-potential were determined (Table 1).

These two parameters correlate with important features of solid biocatalysts such as colloidal stability and size distribution in the corresponding dispersant. By selecting the preparations with optimal properties, a robust solid biocatalyst could be developed with improved physico-chemical properties for further upscaling. ζ-potential data indicated that *f*SNPs without enzymes are stable suspension (between −30 and −40 mV interval), while the ζ-potential of the SNPs with bound *Cv*TA changed due to the protein and became less negative (Table 1).[45] The ζ-potential of pure *Cv*TA indicates moderate stability, which is typical for most proteins in the liquid phase.[46,47] As the average particle size of cobalt ion charged SNPs with different linkers were slightly different, the corresponding amino linker has no significant effect on the final size of *f*SNPs. Nevertheless, due to enzyme immobilization, the average size of *f*SNP-*Cv*TAs increased by minimum of 120 nm in all cases, which could be caused by an extensive solvation sheet and enzyme multilayer on the surface. The measured average size of the *Cv*TA (Table 1) correlated with the experimental 3D structure (PDB ID: 6SNU) obtained by X-ray diffraction.

The resulting *Cv*TA-SNPs biocatalysts were then trapped in PLA matrices by emulsion electrospinning technique resulting in the desired nanofibrous composite structure. Once particles were trapped in nanofibers, their composite is often called as a second-generation nanocomposite, which combines the advantageous properties of the two nanocarriers. Due to the immiscibility of PLA with the aqueous enzyme solution, addition of Span™ 40 emulsifier was required enabling the stabilization of the water-in-oil emulsion to reach the desired morphology and providing continuous and reliable fiber formation.[48]

SEM investigation showed the spherical morphology of the functionalized SNPs with homogenous size distribution (Fig-

Table 1. Particle size (d_P) and ζ-potential changes after cobalt ion (Co^{2+}).and *Cv*TA immobilization on silica nanoparticles (*f*SNP) functionalized with different amino linkers (AmL-1, AmL-2, or AmL-3) and Eda.

	d_P [nm]	ζ-potential [mV]
*Cv*TA	7.9 ± 0.7	−10.6 ± 0.29
SNP-AmL-1-Co	276.8 ± 5.4	−40.80 ± 0.72
SNP-AmL-1-Co-CvTA	398.8 ± 9.1	−22.11 ± 0.25
SNP-AmL-2-Co	328.2 ± 7.3	−31.42 ± 0.24
SNP-AmL-2-Co-CvTA	450.4 ± 59.6	−17.34 ± 0.35
SNP-AmL-3-Co	292.7 ± 2.0	−33.12 ± 0.24
SNP-AmL-3-Co-CvTA	463.6 ± 11.9	−18.01 ± 0.20

ure 5a). Compared to the PLA fibers prepared in the presence of Span™40 (HLB 6.7) emulsifier (Figure 5b), the electrospun matrices preserved the uniform fibrous structure when purified *Cv*TA was immobilized on *f*SNP (Figure 5c), as well as after immobilization of enzymes from the cell lysate (Figure 5d). Furthermore, SEM images of higher magnification illustrated that the *f*SNP-*Cv*TA particles were successfully embedded in the PLA fibers despite the slight aggregation observed (Figure 5e,f).

The immobilized biocatalytic activity (U_B', which shows the activity in unit per the mass of *Cv*TA-fSNP in the nanofibrous matrices) of bound *Cv*TA on *f*SNPs and the entrapped enzymes in PLA fibers were also investigated in the reaction of (*S*)-MBA to acetophenone. The U_B' results clearly show an enhanced activity of the entrapped *Cv*TA bound on *f*SNPs compared to the PLA without binding to *f*SNPs (Figure 6a). Furthermore, the negative effect of purification process could be realized by comparing the *UB'* values of the immobilized purified and the cell lysate originated *Cv*TA. Consequently, the isolated enzymes from lysate demonstrate nearly twofold increase in U_B' values. Regarding to the specific enzyme activity U_E (which shows the activity per enzyme content of the immobilized biocatalyst), immobilization of *Cv*TA on *f*NSP (SNP-AmL-2-Co) and in PLA nanofibers provided similar activity; however, in the case of *f*SNP/PLA nanocomposite it remarkably increased. It also should be noted that it surpassed the activity non-immobilized, that is, free *Cv*TA ($U_E = 779 \pm 82$ U g^{-1}), which could be explained by the stabilization effect of the carrier system (Figure 6b). While dimeric *Cv*TA has weak structural stability which strongly relates

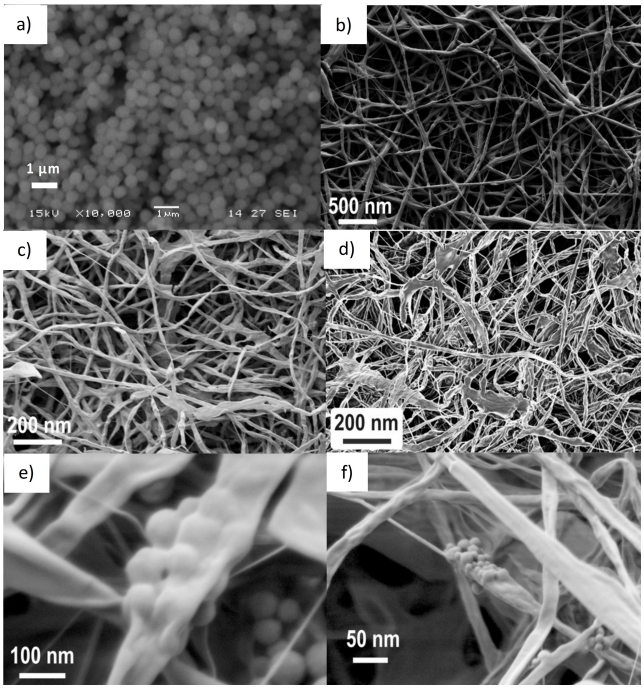

Figure 5. Morphological investigation by using SEM of a) fSNP: SNP-AmL-1-Co, b) PLA nanofibers, c), e) purified CvTA immobilized on fSNP and trapped in PLA nanofibers at different magnification, and d), f) CvTA from the cell lysate immobilized on fSNP and trapped in PLA nanofibers at different magnification.

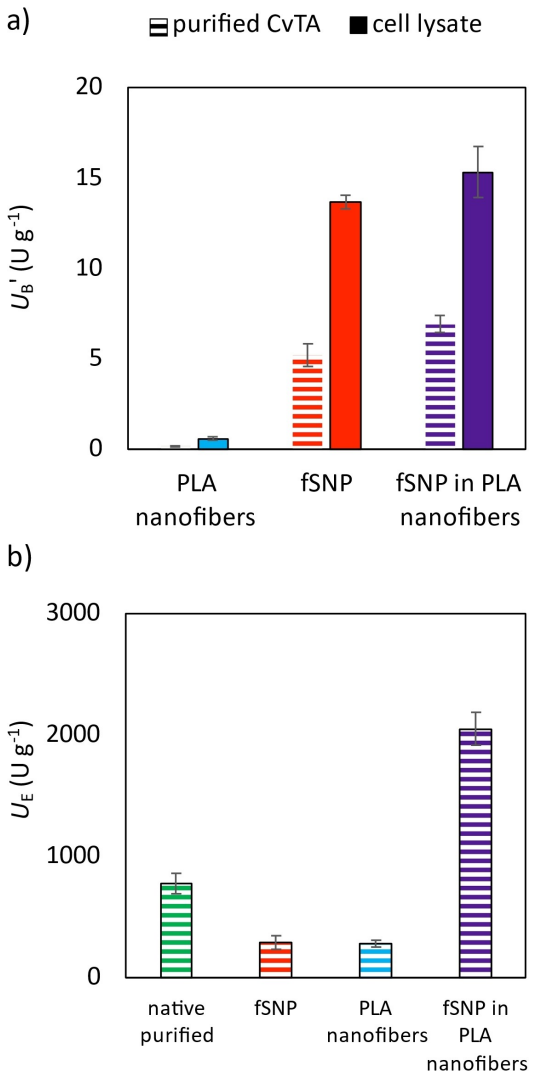

Figure 6. The effect of the applied nanocarrier system (fSNP: SNP-AmL-2-Co, PLA nanofibers and fSNP loaded PLA nanofibers) on a) the biocatalytic activity (UB') of purified CvTA and cell lysate and b) the specific enzyme activity (UE) of purified CvTA.

to its catalytic activity,[49] the simultaneous stabilization of nanoparticles and polymeric chains of nanofibers on the protein structure could be uniquely advantageous.

The stability of an immobilized biocatalyst is a key issue, as it could strongly limit its applications. The enzyme retaining behavior and the reusability of *Cv*TA biocatalysts were also investigated. The enzyme leaching was investigated in order to determine the enzyme loss during the reaction time of 1 h (Figure 7a). The results indicate the stabilizing effect of PLA nanofibers in contrast to the less strong coordinative binding to *f*SNPs, as the 15% loss of enzymes was detected under the same conditions. *Cv*TA immobilized on nanoparticles (fSNPs: SNP-AmL-2-Co) and in composite nanomaterial (*f*SNP in PLA nanofibers) were recycled in the transamination of (*S*)-MBA. After the isolation, washing and incubating with PLP cofactor residual activities were determined. Results with purified enzyme showed, that *Cv*TA attached ton *f*SNP carrier showed

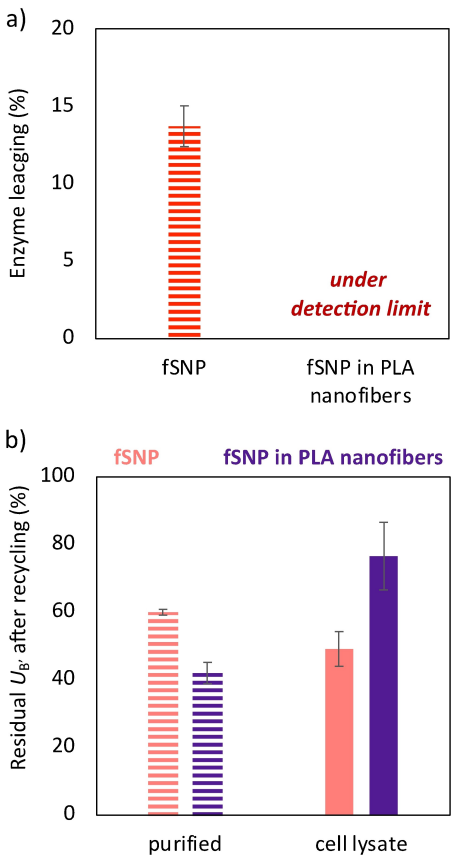

Figure 7. The effect of the applied nanocarrier system (fSNP: SNP-AmL-2-Co, PLA nanofibers and fSNP loaded PLA nanofibers on a) enzyme leaching and b) residual biocatalytic activity (UB') after recycling in the transamination of (*S*)-MBA with pyruvate.

higher remaining activity than in nanocomposite (*f*SNP in PLA nanofibers). However, it is important to note, that the enzyme leaching in the case of simple *f*SNP could influence the results, while enzymes could act on the particle's surface and in soluble (non-immobilized) form simultaneously. In the case of *Cv*TA from cell lysate, nanofibrous composite carrier provided higher residual activity, than the *f*SNP-bounded (Figure 7b). As a conclusion, it can be seen, that cell lysate in nanocomposite had the best reusability, which can be caused by the stabilizing effect of PLA polymeric chains forming a nanostructured layer and some natural components of cell lysate (host proteins, polysaccharides, etc.) which could ensure the natural conditions and environment for the enzyme mimicking the whole cell system.

Raman mapping is a suitable method to investigate the distribution of proteins in the corresponding environment as it is sensitive for the secondary protein structures. The vibrational bands of carbonyl stretching of peptide groups (amide I region) of enzymes (1600–1700 cm^{-1}) showed strong Raman intensity. The Raman spectra of unbound *Cv*TA were used as a reference to localize enzymes in the samples. Thus, their frequency of occurrence is shown in the chemical maps (Figure 8), where the red color indicates the strong existence of proteins, the green areas show a mixed composition, and the blue areas mark the regions of the map with different spectra of other components. In the case of *f*SNP-*Cv*TA-containing samples, the red areas of the maps indicate the successful selective isolation and immobilization of *Cv*TA (Figure 8b-c), compared to the map of pure *f*SNPs without red areas (Figure 8a). Considering the structure of PLA nanofibers in the presence of Span™40 (Figure 6d) was more uniform compared to the PLA prepared without the emulsifier (Figure 8g). The results also revealed that the distribution of native enzyme in PLA matrices is less dispersed, and the entrapment of *Cv*TA from cell lysate in PLA nanofibers indicated more intensive red areas (Figure 8f). This might be the sign of other irrelevant proteins from the crude cell lysate saturating the matrices, opposing the entrapment of purified *Cv*TA in PLA fibers (Figure 8e). Finally, the Raman map of the novel composite systems indicate enhanced distribution of *Cv*TA and well-defined enzyme packages (Figure 6h, i).

Conclusion

In this study, a novel, one-step isolation and immobilization of a recombinant His-tagged variant of a transaminase from *C. violaceum* was successfully demonstrated. *Cv*TA was selectively isolated by using SNPs functionalized with specific affinity linkers charged with metal ions. Based on fine-tuning experiments of SNPs carriers, the AmL-2 amino linker (3-(2-aminoethylamino)propyl]trimethoxysilane) had an acceptable performance in the presence of cobalt ions. Next, uniform, so-called second-generation nanofibrous composite biocatalysts were prepared by entrapping *Cv*TA-containing *f*SNPs in PLA nanofibers through emulsion electrospinning (Figure 9). The *f*SNP-*Cv*TAs in PLA matrices showed biocatalytic activities almost three times higher than those of *Cv*TA coordinated to *f*SNPs and more than ten times higher than those trapped in poly(lactic acid). These results indicate a significant stabilizing effect of fibrous PLA matrices in the case of sensitive recombinant proteins. Furthermore, when performing the immobilization both from purified medium and crude cell lysate, a twofold decrease in the enzymatic activity of purified *Cv*TA enzymes was found. As an advantage, this novel method could offer a promising alternative approach to biotechnologists to reduce costly and time-consuming downstream processes such as multi-step protein isolation and purification. Depending on the target protein and its application, this approach could bring some difficulties as well, for example, the original function of the enzyme can be changed during the combined immobilization procedure. In addition, this method requires specialties, such as the electrospinning machine causing a new step that needs to be optimized, especially in the case of scale-up. However, nanofiber fabrication by electrospinning is a rapidly growing area, thus it is expected to become a robust and generally applicable and available tool in the future. The presented nanocomposite, which combines the positive features of nanoparticles (e.g., huge surface area, good dispersibility and fluency) and nanofibers (e.g., good perme-

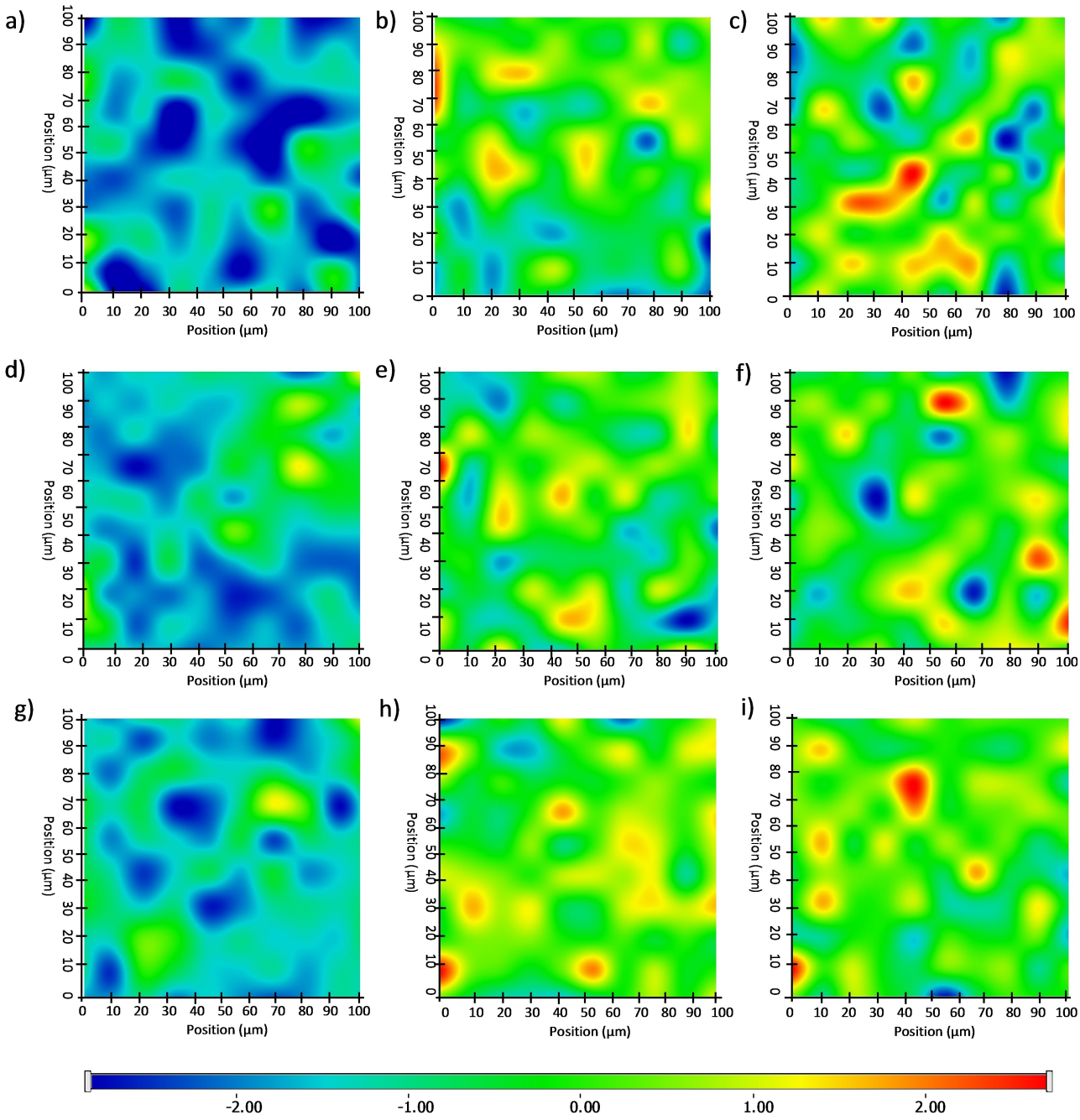

Figure 8. Structural investigation of a) fSNP, b) purified CvTA immobilized on fSNP, c) CvTA from cell lysate immobilized on fSNP, d) PLA nanofibers, e) purified CvTA trapped in PLA nanofibers with Span™ 40, f) CvTA from cell lysate trapped in PLA nanofibers with Span™ 40, g) PLA nanofibers with Span™ 40, h) purified CvTA immobilized on fSNP and trapped in PLA nanofibers with Span™ 40 and i) CvTA from the cell lysate immobilized on fSNP and trapped in PLA nanofibers with Span™ 40 by Raman microscopy (fSNP: SNP-AmL-2-Co). Red: strong existence of CvTA, green: mixed composition, blue: other components than CvTA.

ability and protectivity) could mean a novel tool for the rapidly growing bio-industry.

Experimental Section

Materials and reagents: Propan-2-ol (IPA), hydrogen chloride (cc. aq.), 4-(2-hydroxyethyl)piperazine-1-ethanesulfonic acid) (HEPES), D-(+)-glucose, sodium chloride, sodium phosphate dibasic, potassium phosphate monobasic, tryptone (peptone from casein), yeast extract are the products of VWR (Radnor, PA, USA). (3-Aminopropyl)trimethoxysilane),3[(2-aminoethylamino)propyl]trimethoxysilane-, N^1-(3-trimethoxysilylprop-yl)diethylenetriamine, cobalt chloride hexahydrate, nickel chlorine hexahydrate, sodium pyruvate, pyridoxal 5-phosphate (PLP), (*S*)-(−)-α-methylbenzylamine, Tris(2-carboxyethyl)phosphine) sorbitane monopalmitate (Span™40) were

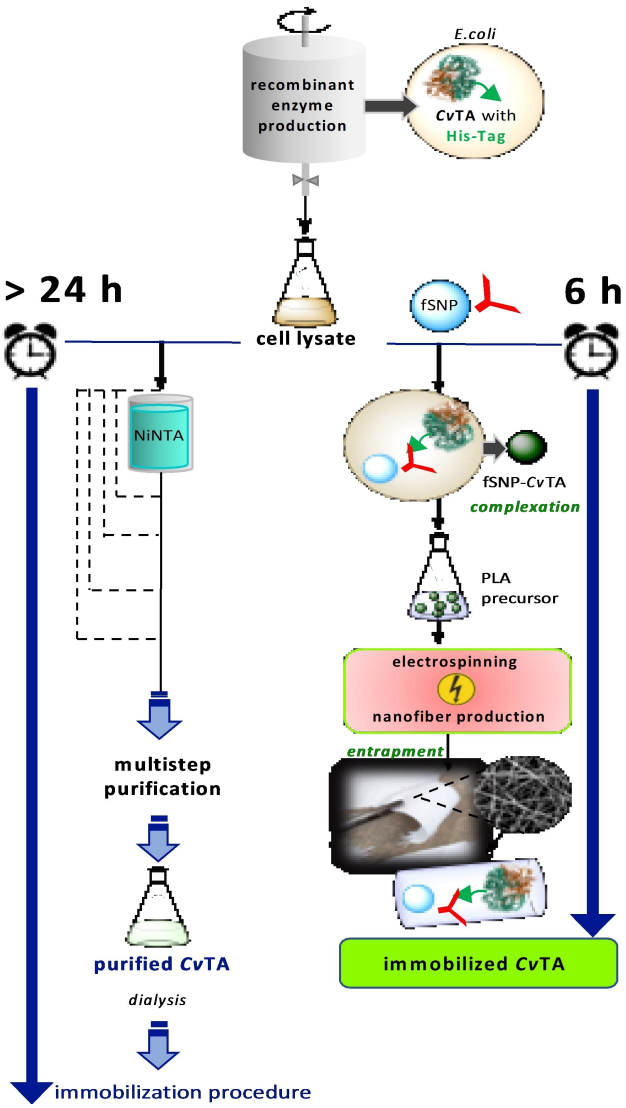

Figure 9. Comparison of a classic isolation, immobilization approach for a recombinant enzymes (transaminase from *C. violaceum*, *Cv*Ta) and the formation of a second-generation nanocomposite system involving silica nanoparticles with affinity functions (*f*SNPs) and embedding *f*SNP-*Cv*TA in PLA nanofibers by electrospinning.

purchased from Sigma-Aldrich. Acetonitrile, absolute ethanol, *N,N*-dimethylformamide (DMF), diethyl ether, dichloromethane (DCM) and ammonium hydroxide (25% aq.) are the products of Molar Chemicals Kft. (Halásztelek, Hungary). Tris(hydroxymethyl)aminomethane (Tris) is the product of TCI (Tokyo, Japan). Lactose monohydrate, acetic anhydride and pyridine were obtained from Merck. Ammonium hydroxide (35% aq.) was the product of Fisher Chemicals (Hampton, NH, USA) Polylactic acid (PLA, Mw = 68000 g mol^{-1}, *dp*: 3–5 mm) was the product of GoodFellow (Cambridge, UK). The ethylenediaminetetraacetic dianhydride (EDa) was synthetized in-house before usage. Milli-Q water ($p > 18.2$ MW cm; Millipore) was used for the preparation of aqueous solutions.

Production and purification of *Cv*TA: The gene of the (*S*)-selective transaminase variant (W60 C) from *C. violaceum* in a pET28a(+) expression plasmid was applied for expression of the protein in *E. coli* BL21(DE3) cells. LB-Kana medium (5 mL; LB medium containing kanamycin, 50 μg mL^{-1}) was inoculated with one fresh colony from an overnight LB-Kana agar plate and cells were grown overnight in shake flask (37 °C, at 200 rpm). Autoinduction medium (250 mL in a 1 L flask; Na_2HPO_4, 6 g L^{-1}; KH_2PO_4, 3 g L^{-1}; tryptone, 20 g L^{-1}; yeast extract, 5 g L^{-1}; NaCl, 5 g L^{-1}; glycerol, 7.56 g L^{-1}; D-(+)-glucose, 0.5 g L^{-1}; lactose, 2 g L^{-1}) was inoculated with seed culture (2 mL) and was shaken for 16 h at 28 °C, 200 rpm. The cells were then harvested by centrifugation (15000 *g*, 4 °C, 20 min). For cell disruption, the harvested cells were suspended in lysis buffer (50 mM HEPES, 20 μM PLP, 2 mM phenylmethylsulfonyl fluoride, 1 mM benzamidine, 1 mM Tris-(2-carboxyethyl)phosphine, pH 7.5). For cells harvested from a 1 L culture, the total amount of 50 mL lysis buffer was used. Lysis was performed by French press method from 1 L culture and the supernatant was separated by centrifugation (20000 *g*, 4 °C, 30 min). The enzyme was purified with immobilized metal affinity chromatography (IMAC) on a Ni-NTA resin (Ni Sepharose® 6 Fast Flow, Merck, Country) and the elution fraction was then dialyzed overnight at 4 °C in 1 L HEPES buffer (50 mM HEPES, 300 mM NaCl, 20 μM PLP, pH 7.5). The dialyzed protein was supplemented with 10 *v/v*% glycerol, frozen rapidly and stored at −80 °C.

Synthesis of functionalized SNPs (*f*SNPs): For the synthesis of silica nanoparticles (SNPs) a modified Stöber method was applied according to our previous study.[50] SNPs (500 mg) were added to absolute ethanol (10 mL) in a well-sealed 20 mL glass vial and the suspension was sonicated for 15 min. Then ammonia solution (50 μL, 25% aq.) was added to the suspension and was shaken for further 10 min at room temperature, 450–600 rpm. Then the corresponding aminosilane agent (1 mmol) was added to suspension and shaking was performed for further 24 h (RT, 450–600 rpm) followed by separation by centrifugation (12000 *g*, 4 °C, 6 min). Then the aminosilane-coated SNPs were washed with ethanol (2× 20 mL), distilled water (1×20 mL) and propan-2-ol (1×20 mL)-applying centrifugation (12000 *g*, 4 °C, 6 min) and decantation after each washing steps-and dried in a vacuum drying chamber (VDL 23, Binder GmbH, Tuttlingen, Germany; at 0.1 mbar) at room temperature overnight.

In a 20 mL, well-sealed, dried and argon-flushed glass vial 200 mg of aminosilane-functionalized SNPs were sonicated in anhydrous *N,N*-dimethylformamide (5 mL) for 10 min. Then, EDa (0.8 mmol) and *N*-ethyl-*N,N*-diisopropylamine (1.6 mmol) were added to the material. The total reaction volume was filled up to 10 mL by addition of the required amount of DMF then flushed with argon. The mixture was shaken for 24 h (60 °C, 450–600 rpm) then 200 μL of distilled water was added to the mixture which was shaken for further 1 h at 60 °C. Finally, the surface-treated SNPs was intensively washed with acetonitrile (3×10 mL), distilled water (1×10 mL) and propan-2-ol (1×10 mL)–applying centrifugation (12000 g, 4 °C, 6 min) and decantation after each washing steps–and dried in a vacuum drying chamber (at 0.1 mbar) at room temperature overnight.

The metal ion complexation of the surface-treated SNPs was performed in 50 mL Falcon tubes. Chelated SNPs (50 mg) were sonicated in distilled water (5.0 mL) for 10 min. After addition of the corresponding metal chloride solution (5 mL, 100 mM), the resulting mixture was shaken at 450–600 rpm, at room temperature for 60 min, followed by separation by centrifugation (12000 g, 4 °C, 6 min). Then the metal-charged *f*SNPs were washed with distilled water (3×10 mL) and propan-2-ol (1 x 10 mL) applying centrifugation (12000 *g*, 4 °C, 6 min) and decantation after each washing steps, and dried in a vacuum drying chamber (at 0.1 mbar) at room temperature overnight.

Immobilization of purified *Cv*TA on *f*SNPs: The immobilization of *Cv*TA was performed in 1.5 mL Eppendorf tubes. 5.0 mg of metal-functionalized SNPs were sonicated in HEPES buffer (500 μL,

50 mM, pH 7.5) for 10 min. The purified *Cv*TA solution was defrosted and added (500 μL) to the proper metal-charged SNPs samples and shaken at 800–1000 rpm, room temperature for 20 min followed by separation by centrifugation (7000 rpm, 25 °C, 2 min). After separation, samples (3 μL, each) were taken from the supernatant binding solution and the absorbance of the samples was measured at 280 nm by Thermo Scientific™ Nanodrop 2000 Spectrophotometer using Protein A280 method. *Cv*TA concentration in samples was determined with the application of extinction coefficient for *Cv*TA (79870 $M^{-1}cm^{-1}$). To characterize the efficiency of the immobilization, the immobilization yield (Y_I) was calculated using the equation $Y_I = c_I \times c_0^{-1}$ where c_I [mg mL^{-1}] is the measured *Cv*TA concentration in the binding solution supernatant, and c_0 [mg mL^{-1}] is the initial *Cv*TA concentration in the binding solution.

Immobilization of *Cv*TA from crude cell lysate on *f*SNPs: The immobilization of *Cv*TA was performed in 1.5 mL Eppendorf tubes. *f*SNPs (5.0 mg) were sonicated in HEPES buffer (500 μL, 50 mM, pH 7.5) for 10 min. The crude cell lysate solution was defrosted and centrifuged (12000 *g*, 10 min, 4 °C). Then the supernatant protein solution (500 μL) was added to the corresponding metal-charged SNPs samples and shaken at 800–1000 rpm, room temperature for 20 min followed by separation by centrifugation (7000 rpm, 25 °C, 2 min). Finally, the immobilized *Cv*TA biocatalysts were washed with HEPES buffer (1 mL, 50 mM, pH 7.5) and were tested directly in the (*S*)-MBA conversion to acetophenone.

Entrapment of *Cv*TA and *f*SNP-CvTA into PLA nanofibers by electrospinning technique: According to the enzyme loading of 0.077 % (where the mass of the enzyme was calculated to the dry mass of PLA in its solution) 50 μL of purified enzyme solution (1.859 mg mL^{-1} *Cv*TA, 20 μM PLP in HEPES 50 mM, pH 7.5), in the case of cell lysate 54 μL (1.719 mg mL^{-1} *Cv*TA, 20 μM PLP in HEPES 50 mM, pH 7.5) or in the case of the *f*SNP-*Cv*TA, enzyme coated particles were suspended in HEPES buffer (100 mg mL^{-1} *f*SNP-*Cv*TA, 50 mM HEPES, pH 7.5, according to the proper particle loading *w/w* % of dry mass of nanofibers) then were mixed with 0.1 mmol of Span™40 for 2 min by a vortex mixer (MIX-28+ Touch Fairy Vortexer, Hangzhou Miu Instruments Co., Ltd., Zheijang, China). Then the mixture was added to 1.00 g PLA solution (8 % *w/w* in DCM/DMF 6 : 1, *v/v*), and it was homogenized for further 2 min by a vortex mixer to get a homogenous precursor mixture. The PLA matrices were prepared by SpinCube Electrospinning machine (Spinsplit Llc, Budapest, Hungary). The precursor mixture was fed to the emitter from a syringe (1.0 mL) at an optimal flow rate (10–25 μL min^{-1}) by a syringe pump. The distance between the collector and the emitter (with 0.7 mm internal diameter) was 10–15 cm. Constant voltage ranging from 10.0 to 15.0 kV was applied to the emitter by using a direct current power supplier. The electrospun samples were dried at room temperature for 1 h, then stored at 4 °C before further application.

Characterization of nanoparticles and nanofibers: The element analysis of functionalized and metal loaded SNPs was investigated by energy dispersive spectroscopy/energy dispersive X-ray analysis (EDS/EDAX with Si(Li) detector) coupled with JEOL JSM-5500LV scanning electron microscope (SEM) applying 20 kV accelerating voltage and sampling time of 60 s. The element composition of the samples was calculated from five parallel measurements.

The morphology of the nanofibrous matrices was analyzed by a [Zeiss LEO 1540 XB FIB/SEM, Jena, Germany] scanning electron microscope (SEM). Samples were placed on a copper grid, then coated with a gold nano-film layer for better imaging by a sputter-coater (Anatech Hummer VI Instrument, Sparks, Nevada, USA) using Ar-plasma, at 10 mA for 180 s.

The particle size distribution of functionalized and enzyme covered SNPs were characterized by dynamic light scattering (DLS), using Malvern Panalitycal ZetaSizer Pro Blue instrument (Worcestershire, UK) equipped with a 633 nm red laser at a detection angle of 173 (back-scattering mode) and a temperature of 25.0 °C. The particles (ca. 5 mg) were sonicated in HEPES buffer (5.0 mL) for 10 min, then analyzed in triplicate.

Raman mapping of nanofiber specimen was performed using a Thermo Fisher DXR Dispersive Raman instrument equipped with a CCD camera and a diode laser operating at a wavelength of 780 nm. Raman chemical map was obtained from a 100 × 100 μm surface of different nanofibers with a step size of 10 μm applying a laser power of 12 mW at 50 μm slit aperture size. Each spectrum of chemical map was recorded with an exposure time of 2 s and acquisition time of 2 s, for a total of 32 scans per spectrum in the spectral range 3300–200 cm-1 with cosmic ray and fluorescence corrections. Each Raman map was normalized in order to eliminate the intensity deviation between the measured areas.

Determination of activity of *Cv*TA: To investigate the biocatalytic activity of *Cv*TA from purified solution or from crude cell lysate, 195 μL of reaction solution (5 mM (*S*)-MBA, 5 mM Na-Pyr, in 50 mM Tris, pH 7.5) and 5 μL of enzyme containing media (purified: 1.859 mg mL^{-1}; lysate: 1.719 mg mL^{-1} *Cv*TA, containing 20 μM PLP in HEPES 50 mM, pH 7.5) were mixed in the vials of a 96-well plate (UV-Star® 96 W microplate, Greiner Bio One GmbH, Kremsmünster, Austria). The specific enzyme activity was calculated by the determination of acetophenone formation at λ = 280 nm for 6 min at 30.0 °C by the "kinetics method" using a Multiskan Sky 96-well plate reader instrument by Thermo Fisher Scientific. In the case of immobilized *Cv*TA (*f*SNP-*Cv*TA, PLA-*Cv*TA or *f*SNP-*Cv*TA/PLA), in a 1.5 mL Eppendorf tubes the corresponding biocatalyst (5.0 mg) was added to the reaction solution (1 mL, 5 mM (*S*)-MBA, 5 mM Na-Pyr, 3.3 uM PLP in 50 mM Tris pH 7.5) and the resulting mixture was shaken at 800 rpm and at 30 °C applying a thermomixer (Eppendorf, ThermoScientific). After 60 min, samples (200 μL, each) were taken from the reaction mixtures and the absorbance of the samples was measured at λ = 280 nm according to the measurements with purified enzyme.

For the investigation of reusability of *Cv*TA biocatalysts, the initial activity of all samples was tested under the same method described above. After the first reaction cycle, samples were washed with Tris buffer (1 mL, 50 mM, pH 7.5) then treated with Tris buffer containing PLP (1 mL, 0.03 mM PLP in 50 mM Tris, pH 7.5) by shaking the mixture at the same conditions for 10 min. Then the enzyme activities were determined as same as in the case of initial activity measurements.

Conversion of the reaction of (*S*)-MBA to acetophenone was determined from the measured concentration of acetophenone at λ = 280 nm by using the Lambert-Beer equation. To characterize the productivity of the biocatalysts, specific biocatalyst activity (U_B, Unit × g^{-1}) and the specific enzyme activity (U_E, Unit × g^{-1}) were calculated using the equation $U_B = n_P \times (t \times m_B)^{-1}$ and $U_E = n_P \times (t \times m_E)^{-1}$ where n_P [μmol] is the amount of the product, *t* [min] is the reaction time, m_B [g] is the mass of the applied immobilized biocatalyst, m_E [g] is the mass of the enyme in the immobilized system. U_B' (Unit × g^{-1}), $U_B = n_P \times (t \times m_{fSNP\text{-}CvTA})^{-1}$, where n_P [μmol] is the amount of the product, *t* [min] is the reaction time, $m_{fSNP\text{-}CvTA}$ [g] is the mass of the *Cv*TA bounded onto functionalized nanoparticles (*f*SNP-*Cv*TA). The activity recovery [%] was calculated from Equation (1):

$$U_{E,\text{immobilized biocatalyst}} \times U_{E,\text{native enzyme}}{}^{-1}) \times 100 \quad (1)$$

Acknowledgements

This research has been supported by the Central Europe Leuven Strategic Alliance (CELSA) through grant CELSA20-24 (B.W.D.) Further support was provided by the National Research Development and Innovation (NRDI) Fund through grant PD-131467 (D.B.W.). B.W.D. acknowledges the János Bolyai Research Scholarship of the Hungarian Academy of Sciences (BO/00175/21) and the ÚNKP-21-5 (ÚNKP-21-5-BME-386) New National Excellence Program of the Ministry of Human Capacities. The research reported in this paper is part of project no. TKP2021-EGA-02, implemented with the support provided by the Ministry for Innovation and Technology of Hungary from the National Research, Development and Innovation Fund, financed under the TKP2021 funding scheme. This work was also supported by a grant of the Romanian Ministry of Education and Research, CCCDI–UEFISCDI, project no. PN-III-P2-2.1-PED-2019-5031, within PNCDI III. The authors thank Dalma Lipták for the preliminary investigation of surface functionalized SNPs. PŽP was financially supported through Grants No. P2-0191, J4-1775 and J4-4562 provided by the Slovenian Research Agency (ARRS).

Conflict of Interest

The authors declare no conflict of interest.

Data Availability Statement

The data that support the findings of this study are available from the corresponding author upon reasonable request.

Keywords: electrospinning · immobilization · nanocomposites · nanoparticles · transaminases

[1] S. Prasad, I. Roy, *Recent Pat. Biotechnol.* **2017**, *12*, 33–56.
[2] A. D. Moreno, D. Ibarra, M. E. Eugenio, E. Tomás-Pejó, *J. Chem. Technol. Biotechnol.* **2020**, *95*, 481–494.
[3] S. Raveendran, B. Parameswaran, S. B. Ummalyma, A. Abraham, A. K. Mathew, A. Madhavan, S. Rebello, A. Pandey, *Food Technol. Biotechnol.* **2018**, *56*, 16–30.
[4] G. Li, J. Wang, M. T. Reetz, *Bioorg. Med. Chem.* **2018**, *26*, 1241–1251.
[5] L. Zhong, Y. Feng, G. Wang, Z. Wang, M. Bilal, H. Lv, S. Jia, J. Cui, *Int. J. Biol. Macromol.* **2020**, *152*, 207–222.
[6] G. K. Meghwanshi, N. Kaur, S. Verma, N. K. Dabi, A. Vashishtha, P. D. Charan, P. Purohit, H. S. Bhandari, N. Bhojak, R. Kumar, *Biotechnol. Appl. Biochem.* **2020**, *67*, 586–601.
[7] S. A. P. Pereira, P. J. Dyson, M. L. M. F. S. Saraiva, *TrAC Trends Anal. Chem.* **2020**, *126*, 115862.
[8] D. Trono, *Advances in Enzyme Technology, Vol. 1* (Ed.: A. Pandey), Elsevier, Amsterdam, **2019**.
[9] B. Wiltschi, T. Cernava, A. Dennig, M. Galindo Casas, M. Geier, S. Gruber, M. Haberbauer, P. Heidinger, E. Herrero Acero, R. Kratzer, C. Luley-Goedl, C. A. Müller, J. Pitzer, D. Ribitsch, M. Sauer, K. Schmöler, W. Schnitzhofer, C. W. Sensen, J. Soh, K. Steiner, C. K. Winkler, M. Winkler, T. Wrienssnegger, *Biotechn. Adv.* **2020**, *40*, 107520.
[10] S. Kulkarni, S. M. Roper, J. M. Stoll, *Biochemical and Molecular Basis of Pediatric Diseases*, 4th ed., (Eds: D. J. Dietzen, E. C. C. Wong, M. J. Bennett), Academic Press, Amsterdam, **2021**.
[11] R. Anjibabu, J. M. R. Boggu, P. Shekhar, B. V. S. Reddy, *Chem. Sel.* **2016**, *1*, 5445–5447.
[12] T. P. Khobragade, S. Sarak, A. D. Pagar, H. Jeon, P. Giri, H. Yun, *Front. Bioeng. Biotechnol.* **2021**, *9*, 926.
[13] G. H. Kim, H. Jeon, T. P. Khobragade, M. D. Patil, S. Sung, S. Yoon, Y. Won, I. S. Choi, H. Yun, *Enzyme Microb. Technol.* **2019**, *120*, 52–60.
[14] M. D. Patil, G. Grogan, A. Bommarius, H. Yun, *Catalysts* **2018**, *8*, 254.
[15] A. I. Freitas, L. Domingues, T. Q. Aguiar, *J. Adv. Res.* **2022**, *36*, 249–264.
[16] L. X. Cai, Y. Q. Lin, Y. M. Chu, X. P. Chen, L. X. Liu, M. Zhang, G. Y. Zhang, *Bio-Protocol* **2022**, *12*, e4282.
[17] J. Tian, R. Jia, D. Wenge, H. Sun, Y. Wang, Y. Chang, H. Luo, *Biotechnol. Lett.* **2021**, *43*, 1075–1087.
[18] H. Ge, X. Liu, H. Yuan, G. Zhang, *Enzyme Microb. Technol.* **2022**, *164*, 110169.
[19] A. C. A. Roque, A. S. Pina, A. M. Azevedo, R. Aires-Barros, A. Jungbauer, G. Di Profio, J. Y. Y. Heng, J. Haigh, M. Ottens, *Biotechnolog. J.* **2020**, *15*, 1900274.
[20] J. C. Chang, Y. A. Chen, S. C. Lin, *Process Biochem.* **2022**, *116*, 108–115.
[21] B. C. de Andrade, A. Gennari, G. Renard, B. D. R. Nervis, E. V. Benvenutti, T. M. H. Costa, S. Nicolodig, N. P. da Silveira, J. M. Chies, G. Volpatoi, C. F. V. de Souza, *Int. J. Biol. Macromol.* **2021**, *184*, 159–169.
[22] A. Gennari, R. Simon, N. D. de Moura Sperotto, C. V. Bizarro, L. A. Basso, P. Machado, E. V. Benvenutti, A. D. C. Viegas, S. Nicolodig, G. Renard, J. M. Chies, G. Volpatoi, C. F. V. de Souza, *Bioresour. Technol.* **2022**, *345*, 126497.
[23] O. T. Gul, I. Ocsoy, *Environ. Technol. Innov.* **2021**, *24*, 101992.
[24] E. Gokturk, I. Ocsoy, E. Turac, E. Sahmetlioglu, *Polym. Adv. Technol.* **2020**, *31*, 2371–2377.
[25] F. D. Koca, D. Demirezen Yilmaz, N. Ertas Onmaz, E. Yilmaz, E. I. Ocsoy, *Biotechnol. Lett.* **2020**, *42*, 1683–1690.
[26] B. Naseer, G. Srivastava, O. S. Qadri, S. A. Faridi, R. U. Islam, K. Younis, *Nanotechnol. Rev.* **2018**, *7*, 623–641.
[27] A. C. Anselmo, S. Mitragotri, J. A. Paulson, *Bioeng. Transl. Med.* **2019**, *5*, e10143.
[28] S. Neethirajan, D. S. Jayas, *Food Bioproc. Technol.* **2011**, *4*, 39–47.
[29] E. Yamamoto, K. Kuroda, *Bull. Chem. Soc. Jpn.* **2016**, *89*, 501–539.
[30] R. K. Kankala, Y. H. Han, J. Na, C. H. Lee, Z. Sun, S. Wang, K. Bin, T. Kimura, Y. S. Ok, Y. Yamauchi, A. Z. Chen, K. C. W. Wu, *Adv. Mater.* **2020**, *32*, 1907035.
[31] Y. Li, N. Li, W. Pan, Z. Yu, L. Yang, B. Tang, *ACS Appl. Mater. Interfaces* **2017**, *9*, 2123–2129.
[32] V. T. Cong, K. Gaus, R. D. Tilley, J. J. Gooding, *Expert Opin. Drug Delivery* **2018**, *15*, 881–892.
[33] A. Liberman, N. Mendez, W. C. Trogler, A. C. Kummel, *Surf. Sci. Rep.* **2014**, *69*, 132–158.
[34] K. K. Sadasivuni, S. Rattan, S. Waseem, S. K. Brahme, S. B. Kondawar, S. Ghosh, A. P. Das, P. K. Chakraborty, J. Adhikari, P. Saha, P. Mazumdar, *Polymer Nanocomposites in Biomedical Engineering* (Eds.: K. K. Sadasivuni, D. Ponnamma, M. Rajan, M. B. Ahmed, M. A. S. A.Al-Maadeed), Springer, Cham, **2019**.
[35] E. Kharlampieva, V. Kozlovskaya, B. Wallet, V. V. Shevchenko, R. R. Naik, R. Vaia, D. L. Kaplan, V. V. Tsukruk, *ACS Nano* **2010**, *4*, 7053–7063.
[36] T. H. Zhou, W. H. Ruan, Y. L. Mai, M. Z. Rong, M. Q. Zhang, *Compos. Sci. Technol.* **2008**, *68*, 2858–2863.
[37] D. H. Lee, C. H. Park, J. M. Yeo, S. W. Kim, *J. Ind. Eng. Chem.* **2006**, *12*, 777–782.
[38] N. Ganesh, R. Jayakumar, M. Koyakutty, U. Mony, S. V. Nair, *Tissue Eng. Part A* **2012**, *18*, 1867–1881.
[39] I. Cacciotti, F. Nanni, *AIP Conf. Proc.* **2016**, *1738*, 270018.
[40] M. Mehrasa, M. A. Asadollahi, K. Ghaedi, H. Salehi, A. Arpanaei, *Int. J. Biol. Macromol.* **2015**, *79*, 687–695.
[41] T. Casalini, F. Rossi, A. Castrovinci, G. Perale, *Front. Bioeng. Biotechnol.* **2019**, *7*, 259.
[42] S. Sato, D. Gondo, T. Wada, S. Kanehashi, K. Nagai, *J. Appl. Polym. Sci.* **2013**, *129*, 1607–1617.
[43] R. Casasola, N. L. Thomas, A. Trybala, S. Georgiadou, *Polymer* **2014**, *55*, 4728–4737.
[44] E. Sánta-Bell, Z. Molnár, A. Varga, F. Nagy, G. Hornyánszky, C. Paizs, D. Balogh-Weiser, L. Poppe, *Molecules* **2019**, *24*, 4146.
[45] E. B. Martínez-Ruiz, F. Martínez-Jerónimo, *Aquatic Toxicol.* **2015**, *169*, 27–36.
[46] G. Genchi, A. Carocci, G. Lauria, M. S. Sinicropi, A. Catalano, *Int. J. Environ. Res. Public Health* **2020**, *17*, 679.

[47] L. Leyssens, B. Vinck, C. Van Der Straeten, F. Wuyts, L. Maes, *Toxicology* **2017**, *387*, 43–56.
[48] S. Bhattacharjee, *J. Controlled Release* **2016**, *235*, 337–351.
[49] N. Schultz, G. Metreveli, M. Franzreb, F. H. Frimmel, C. Syldatk, *Colloids Surf. B* **2008**, *66*, 39–44.
[50] K. Min, J. Kim, K. Park, Y. J. Yoo, *J. Mol. Catal. B* **2012**, *83*, 87–93.
[51] G. Koplányi, E. Sánta-Bell, Z. Molnár, G. D. Tóth, M. Józó, A. Szilágyi, F. Ender, B. Pukánszky, B. G. Vértessy, L. Poppe, D. Balogh-Weiser, *Catalysts* **2021**, *11*, 1149.
[52] T. Börner, S. Ramisch, E. R. Reddem, S. Bartsch, A. Vogel, A. M. W. H. Thunnissen, P. Aldercreutz, C. Grey, *ACS Catal.* **2017**, *7*, 1259–1269.
[53] F. Nagy, E. Sánta-Bell, M. Jipa, G. Hornyánszky, A. Szilágyi, K. László, G. Katona, Cs. Paizs, L. Poppe, D. Balogh-Weiser, *ChemSusChem* **2021**, *15*, e202102284.

Manuscript received: December 2, 2022
Revised manuscript received: January 18, 2023
Accepted manuscript online: January 18, 2023
Version of record online: March 2, 2023